16th World Conference on Earthquake, 16WCEE 2017

Santiago Chile, January 9th to 13th 2017

Paper N° 591

Registration Code: S-V1461451107

SEISMIC PERFORMANCE OF BEAMS WITH HIGH-STRENGTH REINFORCEMENT

D.V. To[1], J.P. Moehle[2]

[1] *Ph.D. Student, Department of Civil and Environmental Engineering, University of California at Berkeley, tovuduy@berkeley.edu*
[2] *Professor, Department of Civil and Environmental Engineering, University of California at Berkeley, moehle@berkeley.edu*

Abstract

An experimental and analytical research program was undertaken to characterize performance of reinforced concrete beams with high-strength reinforcement subjected to reversed cyclic lateral loading. The beams are representative of beams used in special moment frames. In the experimental investigation, two beams reinforced longitudinally with Grade 100 steel having tensile-to-yield strength ratio (T/Y) of 1.18 and 1.30 were tested in the laboratory to study the (a) spread of plasticity, (b) inelastic rotation capacity, (c) buckling characteristics and related requirements for transverse reinforcement, and (d) local bond stress-slip relationship of deformed reinforcing bar anchored in concrete. Transverse reinforcement was Grade 100 steel with T/Y of 1.30. Overall, the two beams achieved rotation capacity of at least 0.035. The beam with lower T/Y of 1.18 failed by fracture of longitudinal bars at base of the beam, while the beam with higher T/Y of 1.30 failed by buckling of longitudinal bars over several hoop spacings. Test data given by strain gauges installed on longitudinal bars clearly showed that beam with higher T/Y achieved greater spread of plasticity compared to the other one. In the analytical study, methods and mathematical models to assess strength and force-displacement response were evaluated based on the experimental results. Two additional beam tests are planned in the present test program.

Keywords: high-strength reinforcement, reinforced concrete beam, special moment frame, spread of plasticity

1. Introduction

There is an increasing demand to use higher-strength reinforcing steel in seismic and non-seismic applications. The main driver for higher-strength reinforcement is the need to reduce bar congestion, material quantities, and construction costs. Even though several mills across the country are able to produce steel bars with yield strength exceeding 60 ksi with relatively high ductility, none of these higher steel grades are able to match the benchmark elongation and strain-hardening properties of Grade 60 A706 steel.

Fig. 1 depicts typical Stress vs. Strain relations of Grade 100 longitudinal and transverse reinforcement used in this experimental program (i.e., Grade 100 with T/Y = 1.18 and T/Y = 1.30). The selected bars have a sharp yield point, a yield plateau, and varying amounts of strain hardening. The T/Y ratios for the Grade 100 bars (1.18 and 1.30) are notably lower than the T/Y ratio of typical ASTM A615 and A706 Grade 60 bars (1.50 and 1.36). Additionally, ultimate uniform elongation of Grade 100 is approximately 8%, which is less than typical values for ASTM A615 and A706 Grade 60 bars (13% and 15%). The lower T/Y ratio is expected to result in reduced spread of plasticity, which, coupled with the lower uniform elongation, is expected to result in lower rotation capacity.

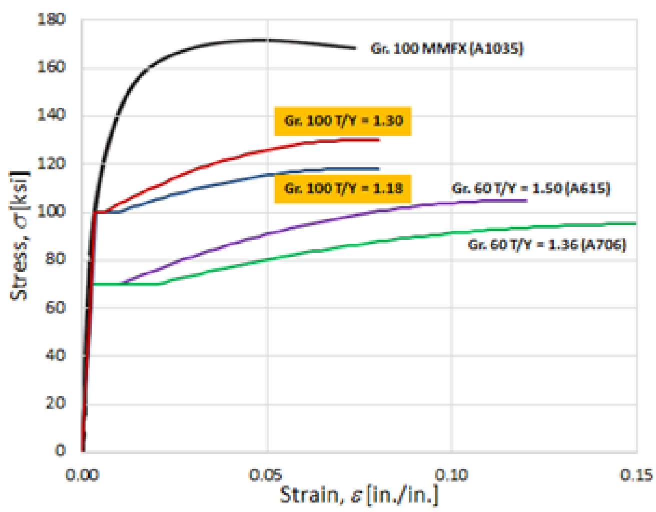

Figure 1: Mechanical properties of Grade 60 and Grade 100 steels

Reinforced concrete Special Moment Resisting Frames (SMRFs) are sometimes used as part of the seismic-force-resisting system in buildings designed to resist earthquake shaking. When subjected to strong earthquake loading, the beams are intended to act as a principal source of inelastic rotation that enables the building frame to deform well into inelastic range. Special proportioning and detailing requirements must be satisfied to enable the frame to resist combinations of shear, moment, and axial force while safely undergoing extensive inelastic deformations as building responds to strong earthquake ground shaking. The detailing requirements for beams using high-strength reinforcement, and the resulting inelastic deformation capacity, are aspects of interest in the present study.

2. Objectives and Scope

The objectives of the research program is to characterize and quantify the seismic performance of reinforced concrete SMRF beams reinforced with Grade 100 reinforcing bars, to develop analytical models of beams with high-strength reinforcement, and to identify the effects on design and performance of buildings using this reinforcement. The objectives are being achieved by designing a laboratory-based research program that will test beams with four different types of reinforcement, specifically A706 Grade 60 reinforcement, A1035 Grade 100 reinforcement without sharp yield plateau, and two Grade 100 reinforcing bars with sharp yield plateaus. Only the last two tests are reported here. The experimental program quantifies the deformation sources, including flexural response (especially spread of plasticity and ultimate rotation), shear response, and bond-slip response. The tests also identify failure modes and detailing requirements. Analytical models of the deformation sources are developed and presented. Studies of the impacts on design and building performance are not presented here. The ultimate goal of the research is to identify conditions and requirements for use of high-strength reinforcement and to initiate code change proposals to permit the use of high-strength reinforcement.

3. Experimental Program

3.1 Specimen Design

Two beams were designed to have cross section and span that are up-scaled (scale factor is 1.5) from a beam specimen previously tested by Ma et al. (1976). That beam had Grade 60 A615 reinforcing bars with T/Y equal to 1.45 (Fig. 2). For the present beam tests, longitudinal reinforcement was Grade 100, one beam with T/Y of 1.18 while the other beam had T/Y of 1.30. Transverse steel, including closed hoops and crossties, were of Grade 100 with T/Y of 1.30 for both beams.

The beams were designed to have relatively low nominal shear stress (approximately $3\sqrt{f_c'}\ psi$), such that shear cracking and deformations, along with the associated effect of increasing tension shift and rotation capacity, would be minimal. The beam designs satisfied confinement requirements of ACI 318 for special moment resisting frame (SMRF) beams, with hoop spacing being reduced to $5d_b$ as recommended (ATC-98, 2014) for higher strength reinforcement with smaller T/Y ratio. Concrete was normal-weight with design compressive strength around 5000 psi. Table 1 summarizes the design and material properties while Figures 2 displays the general design drawings of test specimens in the present research program and in the program reported by Ma et al.

Beam longitudinal bars were embedded in a concrete block with development length calculated in accordance with the seismic provisions of ACI 318 for SMRF beam-column joints. The total anchorage length including the hook was 24 inches.

The beams were cast on their sides with one batch of pre-mixed concrete, resulting in no cold joints. They were covered with wet burlap and plastic, and cured in form for twenty eight (28) days. The forms were removed and the beams were left air dry for another twenty eight days before testing. Full strength of concrete of approximately 5000 psi was achieved on the date of testing (i.e. fifty six days after casting) due to the effects of fly ash used in the concrete design mix.

Table 1: Summary of design and material properties of test specimens

Author	**Ma, Bertero & Popov**	**To & Moehle**	
		Beam 1 T/Y = 1.18	**Beam 2 T/Y = 1.30**
Width (in)	9	13.5	13.5
Height (in)	16	24	24
Length (in)	62.5	93.75	93.75
Depth (in)	14	22.13	22.13
Top & Bottom Reinforcement	4 No. 6	3 No. 8	3 No. 8
Grade	60 (A615)	100	100
$f_y\ (ksi)$	66	104	100
$f_t\ (ksi)$	95	123	124
Tensile-to-yield strength ratio T/Y	1.45	1.18	1.24
Total yield force of top steel (kips)	106	236	236
Scale factor for tensile force		2.23	2.23
$f_c'\ (ksi)$	4	5	5
Transverse reinforcement	4 No. 2	3 No. 4	3 No. 4
Hoop & crosstie spacing (in)	3.5	5	5

Grade	60 (A615)	100	100
$\boldsymbol{f_y}$ $(\boldsymbol{ksi})$	66	100	100
$\boldsymbol{f_t}$ $(\boldsymbol{ksi})$	95	124	124
T/Y ratio	1.44	1.24	1.24
Nominal shear stress	$3.3\sqrt{f_c'}$	$2.9\sqrt{f_c'}$	$2.9\sqrt{f_c'}$

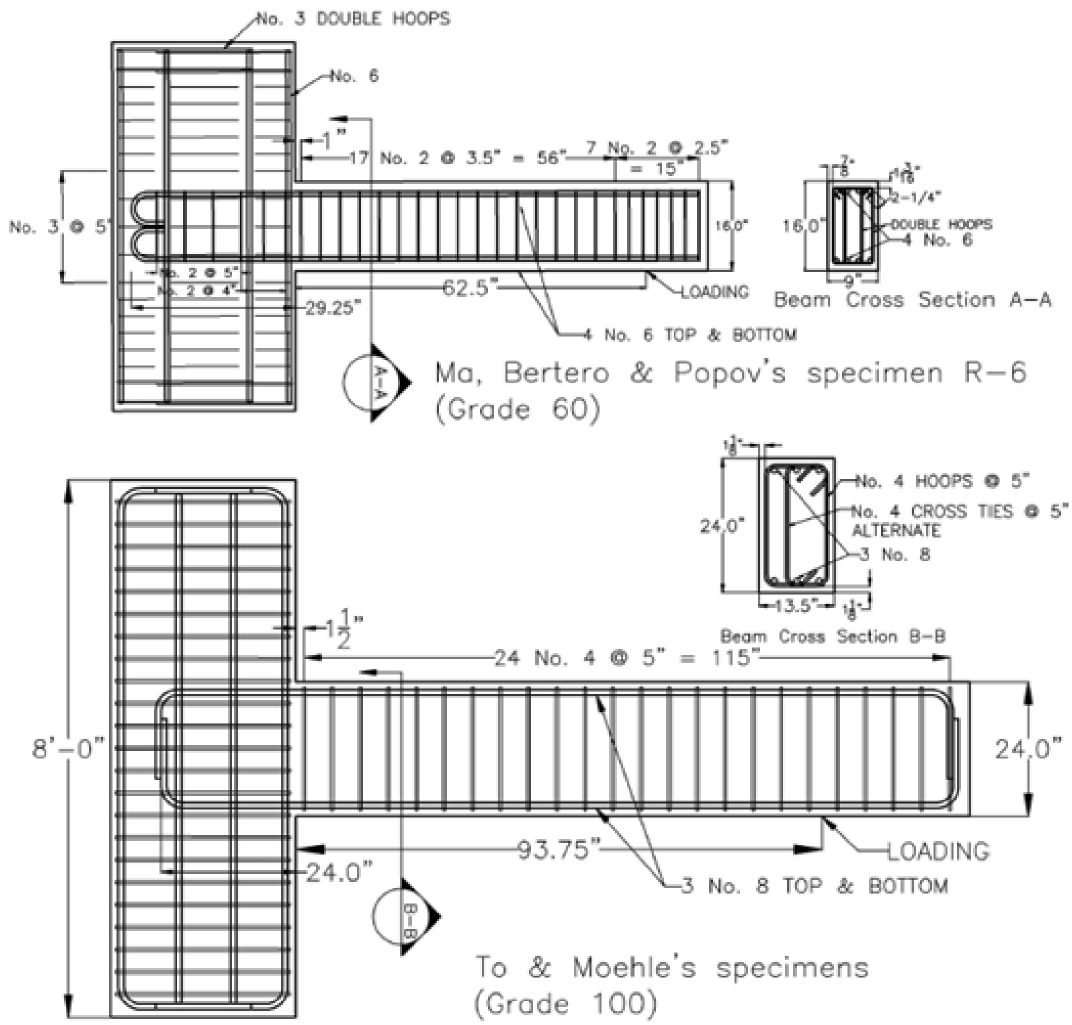

Fig. 2: Details of test specimens

3.2 Test Setup

Cured specimens were oriented vertically and the anchorage block was prestressed to the strong floor of the laboratory (Fig. 3). The prestressing force was designed to prevent uplift and to resist sliding through friction on the interface between test specimen and laboratory floor.

Two actuators were used to apply reversed cyclic lateral forces/displacements to the specimen. The actuators were oriented at a 30-degree angle relative to the intended path of motion of a test beam, such that the actuators could displace the test specimen along the intended path while preventing horizontal movement transverse to the test beam. The actuators had pinned clevises that permitted unrestrained elongation of a test beam along its longitudinal axis.

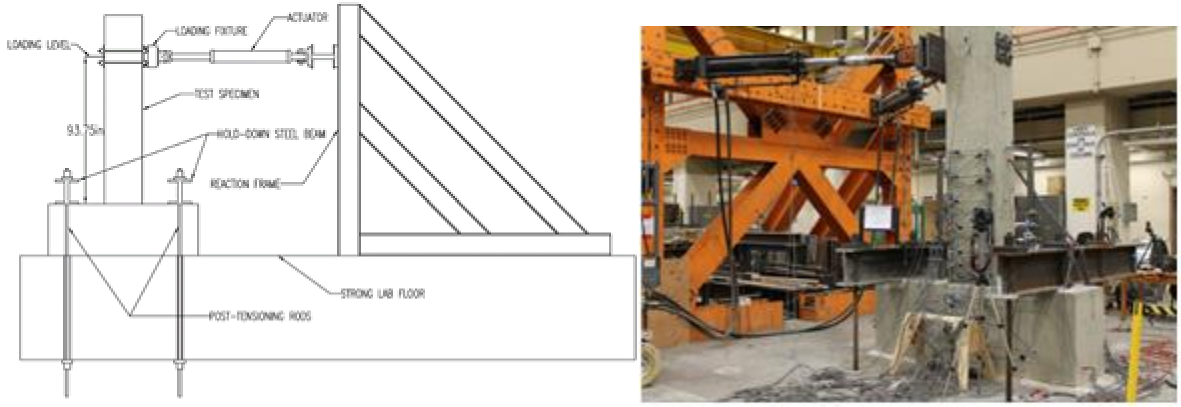

Fig. 3: General test setup

3.3 Instrumentation

Strain gauges were installed on reinforcing bars. Fig. 4 shows typical locations of these strain gauges. These strain gauges were installed to measure strain of longitudinal bars along the beam span and within the anchorage block, as well as to measure strains of hoops and crossties. Linearly Varying Displacement Transducers (LVDTs - Novotechniks) were attached to a test specimen at various locations to measure local deformations, longitudinal bar buckling, slip, beam base sliding (if any) relative to concrete foundation, and beam elongation (Fig. 4).

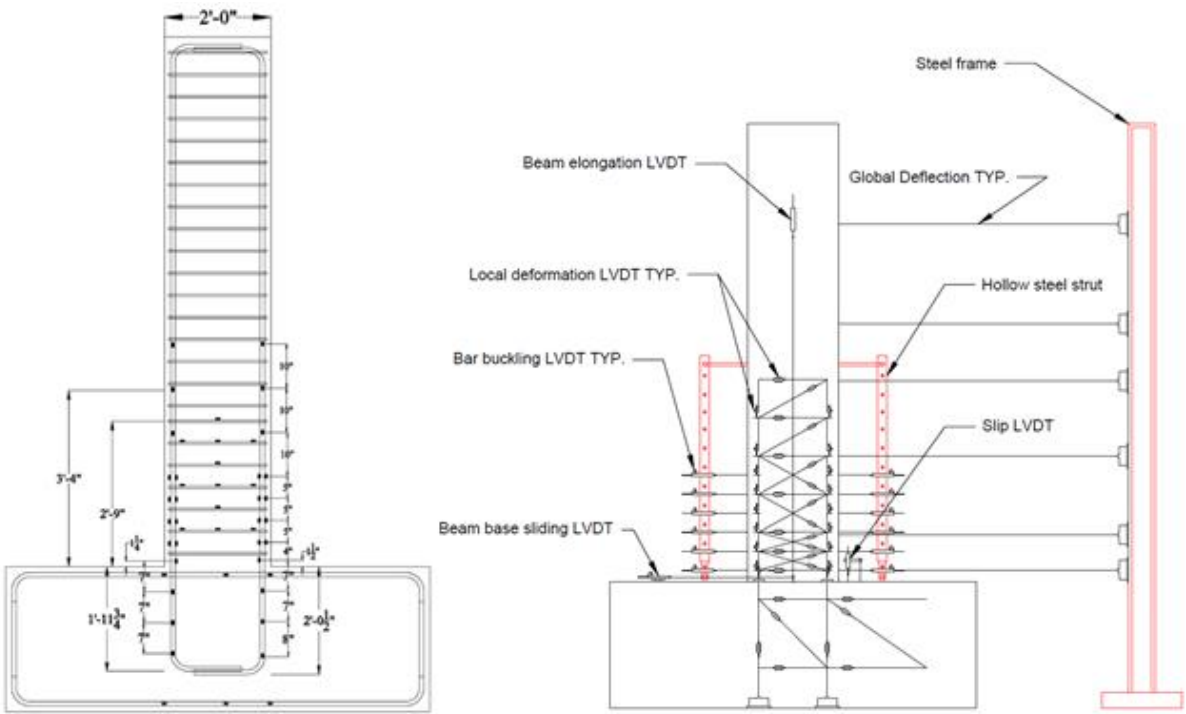

Fig. 4: Instrumentations – Left: strain gauges – Right: displacement transducers.

3.4 Loading Protocol and Procedure

The loading history was developed based on recommendations of FEMA 461 (FEMA, 2007). Initially and up to the onset of yielding, lateral load was applied under force control. Subsequent cycles were applied under displacement control. For cycles having maximum displacements less than 0.02 times beam length, three cycles of loading were applied. For larger displacement amplitudes, only two cycles were imposed. Fig. 5 displays the time series of beam drift ratio measured at the point of lateral force application. At the peak of each cycle, and at the end of a series of cycles, the cyclic loading was paused for recording cracks and other damage.

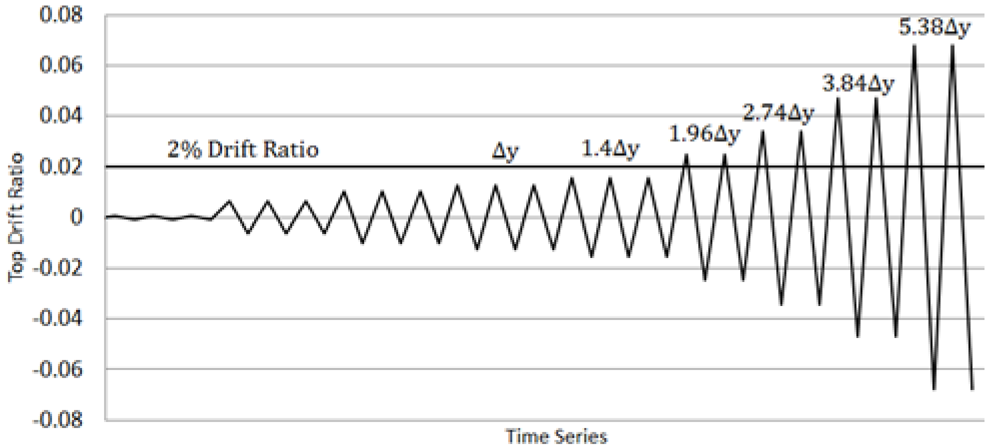

Fig. 5: Loading History

4. Test Results

4.1 General Behavior and Failure Modes

Principal observations on both beams tests are summarized below:

1. Flexural cracks in each of two beams were first observed at loads of approximately 60 percent of yield force. They were similar in either direction of loading.
2. From the beginning of test to the end of loading stage of 1.96Δy, flexural curvature was visible along the beam length. Starting from loading stage of 2.75Δy, major cracks were observed near the fixed end of the beam, leading to concentrated deformations near the fixed end, including concentrated rotation and visible shear distortion.
3. Beam 1 with lower T/Y of 1.18 failed by fracture of the corner longitudinal bar during the second westward loading cycle to 3.84Δy (Fig. 7). During the first cycle to displacement amplitude 5.38Δy, the remaining two longitudinal bars on the same side of the previously fracture bar also fractured.
4. Beam 2 with higher T/Y of 1.30 failed by buckling of all three longitudinal bars over several hoop spacings on the West side of beam when the beam was loaded to the West in the first cycle to displacement amplitude 5.38Δy (Fig. 7). Upon loading to the East direction, the beam twisted noticeably about the beam longitudinal axis.

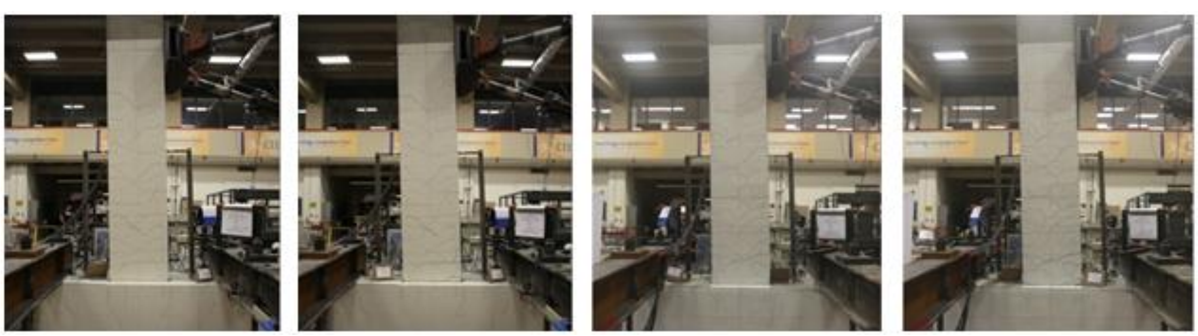

Beam 1 – at 1.96Δy   Beam 1 – at 2.75Δy   Beam 2 – at 1.96Δy   Beam 2 – at 2.75Δy

Fig. 6: Crack development and deflected shape of Beams 1 & 2.

Beam 1 – Failed by fracture of longitudinal bars   Beam 2 – Failed by buckling of longitudinal bars

Fig. 7: Failure mechanism of Beams 1 & 2.

4.2 Spread of Plasticity

Fig. 8 plots the strain profiles of the longitudinal bars along the length of the beams at drift ratio 0.045. As expected, strain was more concentrated at the base and, hence, maximum strains were larger, for the beam with lower T/Y. The maximum strain reached the monotonic strain capacity observed in coupon tests of bare bars, explaining the observed bar fracture.

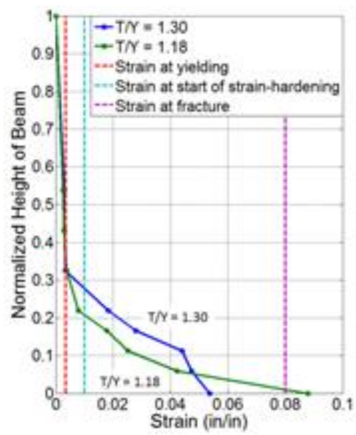

Fig. 8: Strain profile of longitudinal bars at Drift Ratio = 4.5%

4.3 Measured Moment-Drift Ratio Response

Fig. 9 plots the measured relations between moment and drift ratio for the two test beams. Moment is the product of measured actuator force and length from the actuator attachment point and the base of the beam. Drift ratio is the ratio of displacement at the point of actuator attachment and the length from that point to the base of the beam.

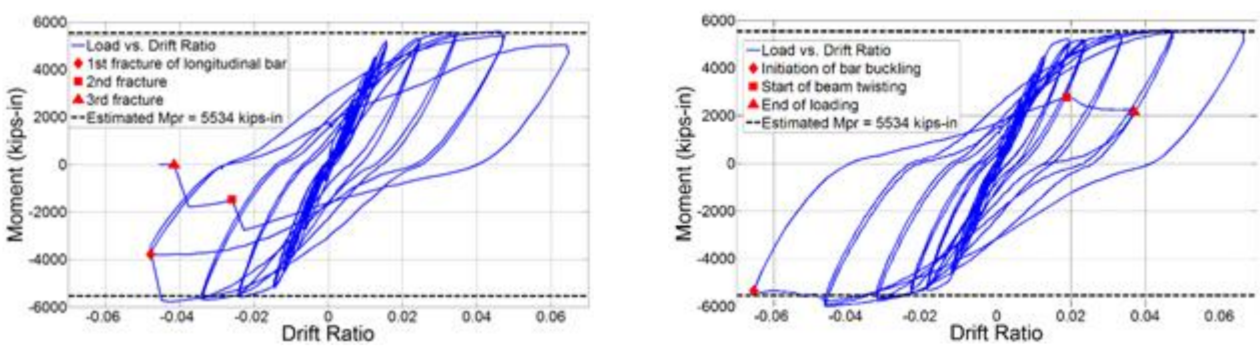

Beam 1 – T/Y = 1.18   Beam 2 – T/Y = 1.30

Fig. 9: Moment vs. Drift Ratio

In order to compare the performance of the test beams of the present testing program and of the Grade 60 test beam reported by Ma et al., the lateral force and deflection values of the present test program were scaled down by the appropriate scaling factor (length scale to the second and the first power, respectively). The scaled results are compared with the measured results from Ma et al. in Fig. 10. Fig. 10 displays the behavior of Beam 1 with T/Y = 1.18 only up to the loading amplitude of 3.84Δy, when the first fracture of a corner longitudinal bar occurred.)

The following observations are made:

1. Prior to yielding, the beams with high-strength reinforcement were less stiff than the beam with Grade 60 reinforcement. This is expected because the beams with high-strength reinforcement have lower reinforcement ratio than the beam with Grade 60 reinforcement.
2. The yield strengths of all three beams were essentially equal. This is expected because the scaled values of the quantity $A_s f_y$ were the same for all three beams.
3. Strain-hardening in the load-displacement relation increased as the T/Y ratio increased. Alternatively stated, the greater strain-hardening in the stress-strain relation of the reinforcement was reflected in greater strain-hardening in the load-displacement relation.
4. The high-strength beams achieved displacement capacity at least equal to the displacement capacity of the Grade 60 beam. This result was unexpected and has not been explained at the time of this writing. Additional testing of a beam with A706 Grade 60 reinforcement is planned to further explore this observation.

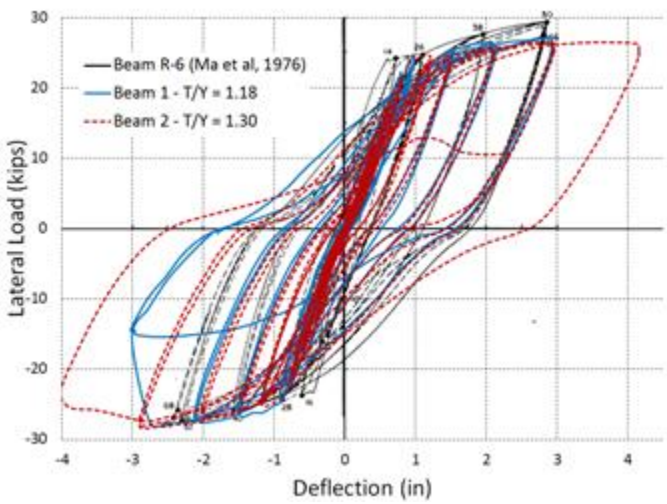

Figure 10: Gr. 60 Beam vs. Gr. 100 Beam

4.4 Deformation Components

It is of interest to separate the total deformation into three major components, which are flexural, shear, and slip components. Global deflection was measured by wire potentiometers, while local deformation was measured by LVDTs attached in a grid over the test specimen (Fig. 4). Considering the LVDT measurements as the real deformations of a truss, the principle of virtual forces can be used to identify the contributions of the individual components to the global displacement. For this purpose, flexural deformation is defined as the deformation due to elongation or shortening of the longitudinally oriented LVDTs. Shear deformation is defined as the deformation measured diagonally and transversely by the LVDTs. The bottom two longitudinal LVDTs measure both flexural deformation and slip of longitudinal reinforcement out of the anchorage. Therefore, another set of LVDTs was used to measure slip of reinforcement separately and subtract that from the bottom two LVDTs to estimate the flexural deformation associated with those LVDTs without the slip contribution.

The LVDTs measure local deformations extended up from the anchorage block to an elevation 52.5 inches above anchorage block. Deformation of the remaining length of the beam up to loading point was calculated based on elastic theory of mechanics.

Fig. 11 shows the force-lateral displacement relations separated into flexure, shear, and slip components for Beam 2 with T/Y = 1.30. Fig. 12 shows the percentage contribution of each component to the total deformation. Results for Beam 1 were similar but are not presented here. For both tests, shear deformation contributed roughly 5-8% of the total deflection at the loading point. Slip of longitudinal bars from the anchorage block contributed as much as 30-40% of the total deflection. The percentage contribution from slip was somewhat higher for Beam 1, probably because the lower T/Y ratio for that beam resulted in smaller spread of plasticity and, consequently, smaller total flexural contribution. The remaining deformation was due to flexure, which was dominant for both beams.

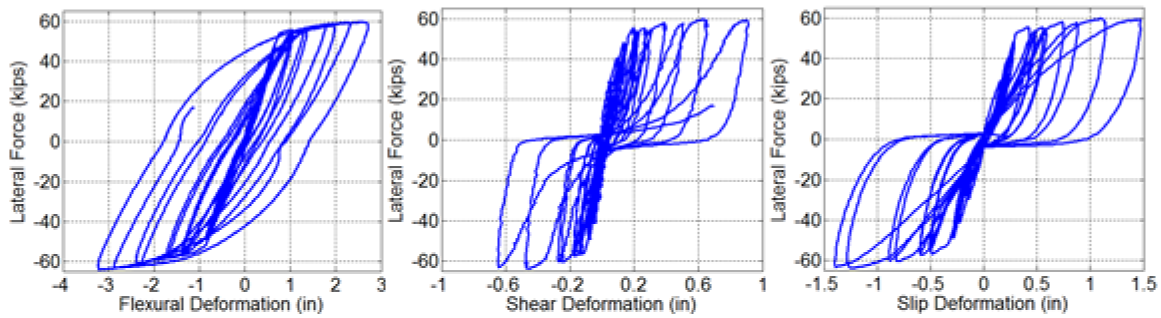

Fig. 11: Flexural, shear, and slip behaviors – Beam 2 – T/Y = 1.30

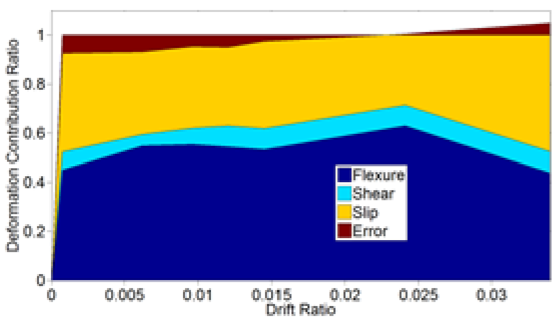

Beam 1 – T/Y = 1.18

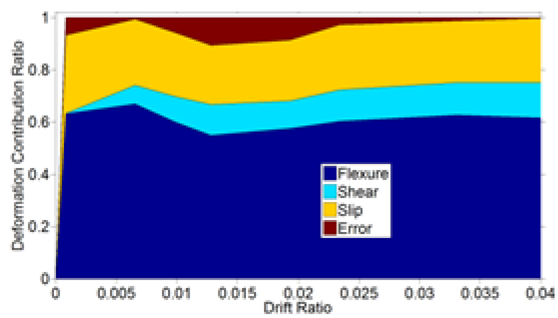

Beam 2 – T/Y = 1.30

Fig. 12: Contribution of major deformation components

5. Analytical OpenSees Models

Analytical models of the test beams were implemented in OpenSees. Fig. 13 depicts the modeling components. The overall model has a distributed plasticity force-based beam-column element to simulate flexure and shear by the use of section aggregator, and a zero-length section element to model rotations due to bar slip response (Fig. 13). Details of the different component models are described in the following text.

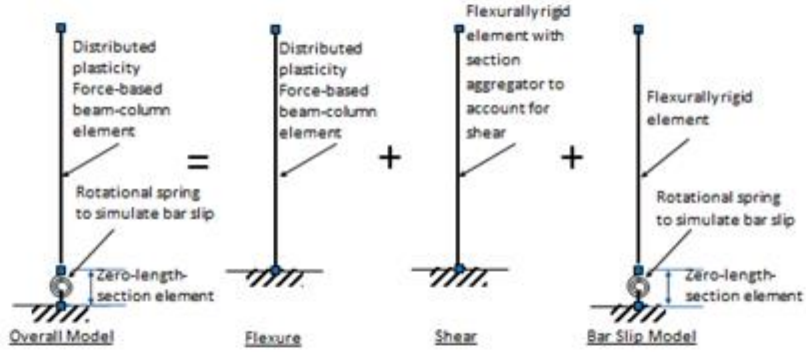

Fig. 13: Overall OpenSees model of test beams

5.1 Flexural Model

Flexural response of the test beams is modelled by using distributed plasticity force-based beam-column element with four Gauss-Lobatto integration points including two points at ends of beam to account for locations of largest moment and curvature (Fig. 14). A fiber section is used for the beam-column element with cover and core concrete having properties described by the algebraic form proposed by Mander at al. (1988a). The steel fiber, on the other hand, has cyclic properties according to the Giuffre-Menegotto-Pinto model (Filippou et al. 1983). The flexural cyclic behavior simulated by the model is compared against that from the test data in Fig. 14.

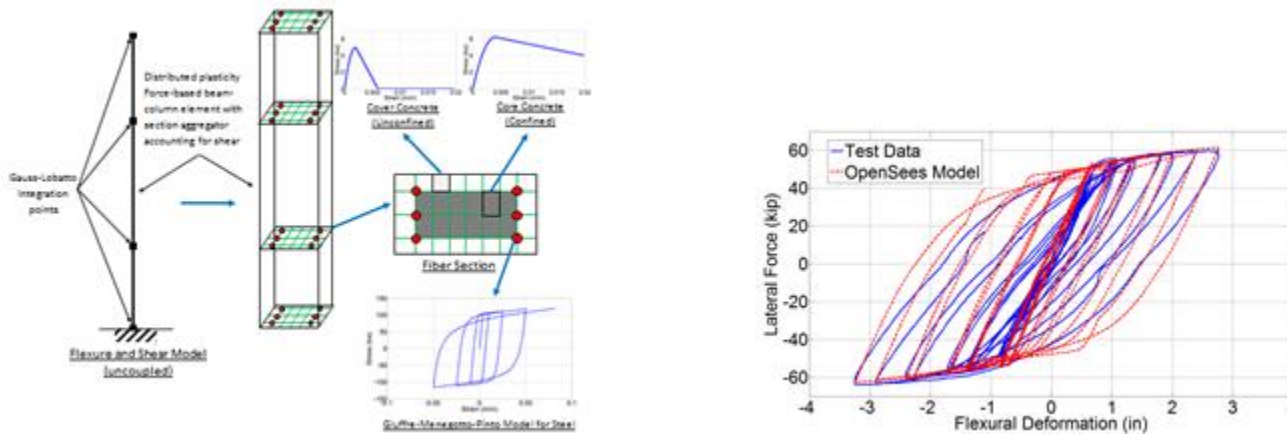

Fig. 14: Flexural model and response

5.2 Shear Model

It is common in design-office practice to model shear behavior using linear-elastic properties of the gross section, with cracking effects perhaps introduced through a stiffness reduction factor. In this case, flexure and shear are uncoupled within the element. The upper right plot of Fig. 15 compares the measured shear deformations with the linear properties obtained by calibrating linear initial stiffness such that they correlate well. Apparently, shear deformations are coupled to flexural response, such that, once flexural yielding occurs, inelastic response in shear is also observed, result in poor comparison between measured and calculated shear response.

To improve the correlation, a Modified Ibarra-Medina-Krawinkler Deterioration Model with Pinched Hysteretic Response (MIMK) was implemented. The comparison with the measurements (lower right of Fig. 15) is greatly improved, although it must be admitted that the parameters of the Ibarra model were selected after the fact to obtain the best correlation.

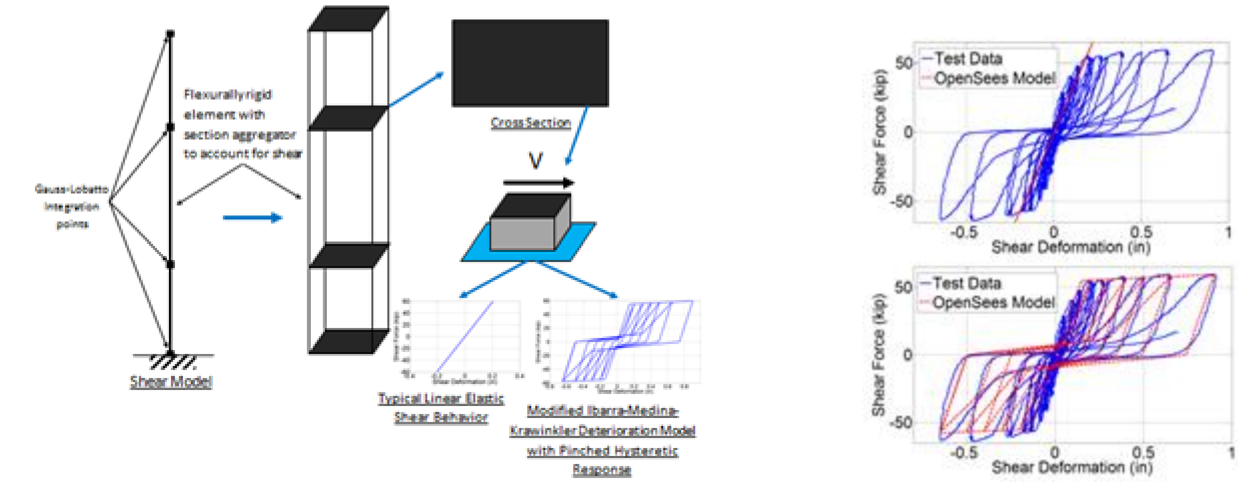

Fig. 15: Shear model and response. Top right corner: Linear elastic shear response; Bottom right corner: shear response using Modified Ibarra-Medina-Krawinkler model

5.3 Slip Model

It is common in design-office practice to model effects of slip either by adding a linear slip spring or, more commonly, by reducing the stiffness of the flexural spring in the linear range by using a stiffness reduction factor. The upper right plot of Fig. 16 compares the measured slip deformations with the linear slip spring that has linear stiffness adjusted to produce comparable fit against test data.

An improved model to estimate hysteretic response of bar slip involves constructing fiber section and assigning its properties to the zero-length section element (Fig. 16). The fiber section has cover and core concrete properties similar to those described in flexural element. The hysteretic model by Zhao and Sritharan (2007) is adopted to describe the cyclic response of the steel fiber in the fiber section. In this implementation, stress and slip at yielding and ultimate were taken from the test data. A zero-length section element, which actually has unit length implicitly, is used for section analysis to calculate the moment-rotation response. The behavior of rotational spring is calibrated to have initial stiffness and hysteretic response that is similar to the measured slip response of the test beams. The behavior of slip from models and test data are presented in Fig. 16.

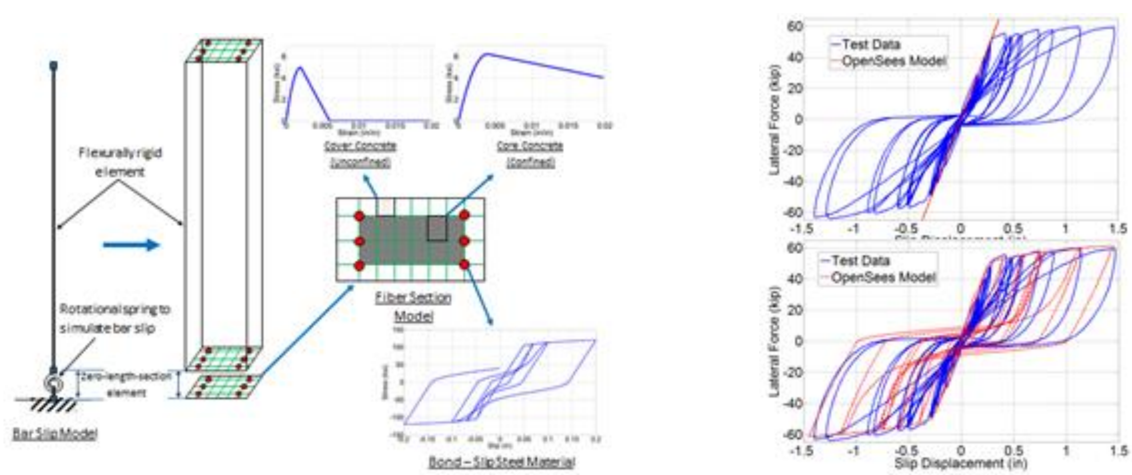

Figure 16: Slip model and response. Top right corner: Linear elastic slip response; Bottom right corner: slip response using fiber section and steel fiber properties by Zhao & Sritharan

5.4 Overall Model Response

Three versions of the analytical model were developed and subjected to the displacement history measured during a test. The comparison of the calculated and measured load-displacement relations provides information on the importance of including various components in the overall analytical model (Fig. 17).

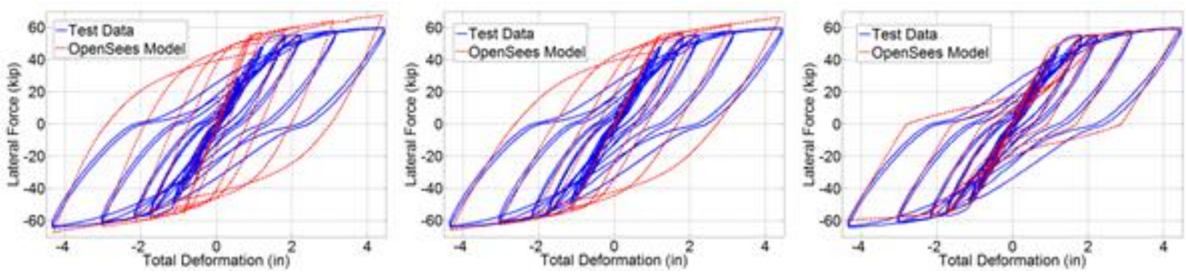

Fig. 17: Overall Response of OpenSees Models. Left: Inelastic Flexure and Elastic Shear; Middle: Inelastic Flexure, Elastic Shear and Slip; Right: Inelastic Flexure, Shear by Modified Ibarra-Medina-Krawinkler Model, and Slip by fiber section with bond-slip steel model by Zhao and Sritharan.

Fig. 17a presents results for an analytical model that considers inelastic flexure and elastic shear. Although the strength (which is limited by flexural strength) is well modeled, the initial stiffness is overestimated and the shapes of the load-displacement loops are wider than those of the test beam, which indicates excessive energy is being dissipated by the analytical model.

Fig. 17b presents results for an analytical model that considers inelastic flexure, elastic shear, and elastic slip. By including slip, the analytical model produces a better match to the measured stiffness. However, the shape of the load-displacement relation is still too wide.

Fig. 17c presents results for an analytical model that considers inelastic flexure, shear, and slip, as described previously. This model produces the best hysteretic response as it matches the initial stiffness, inelastic lateral strength, and load reversal behavior of the test beam reasonably well throughout the entire deformation history.

6. Summary and Conclusion

There is an increasing demand to use higher-strength reinforcing steel in seismic and non-seismic applications. Research is needed to better understand the design requirements for structures using high-strength reinforcement. An experimental and analytical research program was undertaken to characterize and quantify the seismic performance of special moment frame concrete beams reinforced with Grade 100 reinforcement. Results for two beams tested under reversed cyclic loading are reported.

The test results indicated that beams reinforced with Grade 100 reinforcement can achieve performance nearly equivalent to that obtained using conventional Grade 60. A beam with T/Y of 1.18 failed at loading cycle of amplitude of 4.5% drift ratio by fracture of the longitudinal bars. A second beam with higher T/Y of 1.30 failed when loaded to 6.5% drift ratio by buckling of the longitudinal bars over several hoop spacings. The beam with higher T/Y had greater spread of plasticity than the beam with lower T/Y, leading to the higher inelastic rotation capacity.

An analytical model incorporating effects of flexure, shear, and slip was implemented. A model incorporating inelastic flexure with elastic shear and slip properties was able to model the initial stiffness and strength, but the overall shape of the hysteresis was not well modeled. A model including inelastic response in flexure, shear, and slip produced better overall hysteresis.

5. References

[1] ACI 318 (2014). Building Code Requirements for Structural Concrete (ACI 318-14) and Commentary, American Concrete Institute, Farmington Hills, MI.

[2] ATC 98, 2014. *Use of High-Strength Reinforcement in Earthquake-Resistant Concrete Structures*, ATC-98 Report, Applied Technology Council, Redwood City, California, 231 pp.

[3] Berry, M.P., D.E. Lehman, and L.N. Lowes (2008). "Lumped-Plasticity Models for Performance Simulation of Bridge Columns," *ACI Structural Journal*, Vol. 105, No. 3, pp. 270-279.

[4] Elwood, K.J., and M.O. Eberhard (2009). "Effective Stiffness of Reinforced Concrete Columns," *ACI Structural Journal*, Vol. 106, No. 4, pp. 476-484.

[5] FEMA 461, 2007. Interim Testing Protocols for Determining the Seismic Performance Characteristics of Structural and Nonstructural Components, Federal Emergency Management Agency, Washington, D.C., 138 pp.

[6] Filippou, F.C., Popov, E.P., Bertero, V.V. (1983). *Effects of Bond Deterioration on Hysteretic Behavior of Reinforced Concrete Joints*. Report EERC 83-10, Earthquake Engineering Research Center, University of California, Berkeley.

[7] Hognestad, E. (1951*). A Study of Combined Bending and Axial Load in Reinforced Concrete Members*, Bulletin 399, University of Illinois Engineering Experiment Station, Urbana, Ill., 128 pp.

[8] Ibarra L.F., Medina R.A., and Krawinkler H. (2005). "Hysteretic Models That Incorporate Strength and Stiffness Deterioration," *Earthquake Engineering and Structural Dynamics*, 34(12), 1489-1511.

[9] Lehman, D.E., and Moehle, J.P. (2000). *Seismic Performance of Well-Confined Concrete Columns*. UCB/PEER 1998/01, Pacific Earthquake Engineering Research Center, Berkeley, California.

[10] Ma, S-Y.M., V.V. Bertero, and E.P. Popov (1976). *Experimental and Analytical Studies on Hysteretic Behavior of Reinforced Concrete Rectangular and T-Beams*, Report No. UCB/EERC 76/2, University of California, Berkeley, CA, 241 pp.

[11] McKenna, F., Fenves, G.L., Scott, M.H., and Jeremic, B., 2000. Open System for Earthquake Engineering Simulation (OpenSees) [software]. Pacific Earthquake Engineering Research Center, University of California, Berkeley, CA. <http://opensees.berkeley.edu>

[12] Mander, J.B., M.J.N. Priestley, and R. Park (1984). *Seismic Design of Bridge Piers*, Report 84-02, Department of Civil Engineering, University of Canterbury, Christchurch, New Zealand.

[13] Mander, J.B., Priestley, M.J.N., and Park, R. (1988a). "Theoretical Stress-Strain Model for Confined Concrete," *Journal of Structural Engineering*, Vol. 114, No. 8, pp. 1804-1826

[14] Mander, J.B., Priestley, M.J.N., and Park, R. (1988b). "Observed Stress-Strain Behavior of Confined Concrete," *Journal of Structural Engineering*, Vol. 114, No. 8, pp. 1827-1849

[15] Moehle, J. P. (2014). *Seismic Design of Reinforced Concrete Buildings*, Mc Graw-Hill Education, New York, 760 pp.

[16] Neuenhofer, A., and Filippou, F.C. (1997). "Evaluation of Nonlinear Frame Finite-Element Models." *J. Struct. Eng.*, 123(7), 958-966

[17] Priestley, M.J.N., and R. Park (1987). "Strength and Ductility of Concrete Bridge Columns under Seismic Loading," *ACI Structural Journal*, Vol. 84, No. 1, pp. 61-76.

[18] Razvi, S., and M. Saatcioglu (1999). "Confinement Model for High-Strength Concrete," *Journal of Structural Engineering*, Vol. 125, No. 3, pp. 281-289.

[19] XTRACT (2009). XTRACT, version 3.0.8. TRC/Imbsen Software Systems, http://www.imbsen.com/xtract.htm.

[20] Zhao, J., and S. Sritharan (2007). "Modeling of Strain penetration Effects in Fiber-Based Analysis of Reinforced Concrete Structures," *ACI Structural Journal*, 104(2), pp. 133-141.